

# Hyper-X Stage Separation Wind-Tunnel Test Program

William C. Woods,\* Scott D. Holland,† and Michael DiFulvio‡  
NASA Langley Research Center, Hampton, Virginia 23681-2199

NASA's Hyper-X research program was developed primarily to flight demonstrate a supersonic combustion ramjet engine, fully integrated with a forebody designed to tailor inlet flow conditions and a free expansion nozzle/afterbody to produce positive thrust at design flight conditions. With a point-designed propulsion system the vehicle must depend on some other means for boost to its design flight condition. Clean separation from this initial propulsion system stage within less than a second is critical to the success of the flight. This paper discusses the early planning activity, background, and chronology that developed the series of wind-tunnel tests to support multi-degree-of-freedom simulation of the separation process. Representative results from each series of tests are presented, and issues and concerns during the process and current status are highlighted.

## Nomenclature

|                |  |
|----------------|--|
| $A_{sep}$      | = first Euler angle, taken about Hyper-X Research Vehicle (HXRV) $y$ axis, positive Pegasus/adaptor nose up relative to the HXRV, deg  |
| $B_{sep}$      | = second Euler angle, taken about HXRV $z$ axis, positive Pegasus/adaptor nose right relative to the HXRV, deg   |
| $b_{ref}$      | = Hyper-X vehicle reference span (5.19 ft)   |
| $C_m$          | = pitching-moment coefficient (pitching moment/ $q_\infty S_{ref} l_{ref}$ )   |
| $C_{sep}$      | = third Euler angle, taken about HXRV $x$ axis, positive Pegasus/adaptor right wing down relative to the HXRV, deg   |
| $l_{ref}$      | = Hyper-X vehicle reference length (12.0 ft)   |
| $q_\infty$     | = freestream dynamic pressure, psf   |
| $S_{ref}$      | = Hyper-X vehicle reference area (36.144 ft <sup>2</sup> )   |
| $x_{sep}$      | = axial separation distance, measured in the HXRV coordinate system between the moment reference point of the Pegasus/adaptor and the moment reference point of the Hyper-X Launch Vehicle (HXLV), positive forward, in. |
| $y_{sep}$      | = lateral separation distance, measured in the HXRV coordinate system between the moment reference point of the Pegasus/adaptor and the moment reference point of the HXLV, positive right, in.                          |
| $z_{sep}$      | = vertical separation distance, measured in the HXRV coordinate system between the moment reference point of the Pegasus/adaptor and the moment reference point of the HXLV, positive down, in.                          |
| $\alpha$       | = angle of attack, deg   |
| $\beta$        | = angle of sideslip, deg   |
| $\delta_{elv}$ | = elevon (symmetric horizontal tail) deflection, deg   |

## Introduction

THE Hyper-X Research Vehicle (HXRV, or free flyer) (Fig. 1) is a 12-ft-long, 2700-lb technology demonstrator designed

Presented as Paper 2000-4008 at the AIAA 18th Applied Aerodynamics Conference, Denver, CO, 14–17 August 2000; received 26 October 2000; revision received 4 January 2001; accepted for publication 5 July 2001. Copyright © 2001 by the American Institute of Aeronautics and Astronautics, Inc. No copyright is asserted in the United States under Title 17, U.S. Code. The U.S. Government has a royalty-free license to exercise all rights under the copyright claimed herein for Governmental purposes. All other rights are reserved by the copyright owner. Copies of this paper may be made for personal or internal use, on condition that the copier pay the \$10.00 per-copy fee to the Copyright Clearance Center, Inc., 222 Rosewood Drive, Danvers, MA 01923; include the code 0022-4650/01 \$10.00 in correspondence with the CCC.

\*Aerospace Engineer, Aerothermodynamics Branch, MS 408A. Associate Fellow AIAA.

†Assistant Branch Head, Aerothermodynamics Branch, MS 408A. Senior Member AIAA.

‡Facility Manager and Safety Head, Aerothermodynamics Branch, MS 408A. Member AIAA.

to flight demonstrate for the first time a fully airframe-integrated scramjet propulsion system. The lower surface of the forebody is designed to tailor the engine inlet inflow and the lower surface of the afterbody serves as the expansion nozzle for the exhaust plume. This airframe, based on previous research activities and follow on contractual studies<sup>1–4</sup> to integrate efficiently with a scramjet propulsion system, is shown in three views in Fig. 2. Figure 3 illustrates the nominal trajectory for the Hyper-X flight experiment. The Hyper-X Launch Vehicle (HXLV) stack will be carried to 20,000 ft under the wing of a B-52 in captive/carry flight. The HXLV will be dropped at this altitude, the Pegasus ignited, and the assembly accelerated to the desired test Mach number (Mach 7 for first and second flight, Mach 10 for third flight) and dynamic pressure ( $q_\infty = 1000$  psf). When the stack reaches test conditions and attitude, a stage separation sequence of events separates the free flyer from the booster, the engine experiment is conducted, and the research vehicle follows a preprogrammed controlled deceleration trajectory to splash down in the ocean. Although occurring in less than 500 ms, stage separation is critical to reach engine test point and hence critical to mission success. A complete aerodynamic characterization of stage separation requires at least four components: pre-separation HXLV aerodynamics, mutual interference aerodynamics of the HXRV in close proximity with the booster, post-separation (interference-free) booster aerodynamics, and post-separation (interference-free) HXRV aerodynamics. Thus, any discussion of this program, the challenges faced, the successes, the failures, and the current status cannot be adequately addressed without discussion of the launch vehicle, research vehicle, and overall aerodynamic database,<sup>5,6</sup> which are all intertwined with the stage separation. This paper highlights the chronology of the wind-tunnel test program for risk reduction of the stage separation event.

## Chronology

The HXRV requires a booster to deliver it to engine test point, which for first flight is  $M_\infty = 7$ ,  $q_\infty = 1000$  psf, at an altitude of approximately 95,000 ft. The first candidate booster to be evaluated was the Castor IVb. An interstage adapter (Fig. 4) was designed to mate the nonaxisymmetric HXRV to the cylindrical booster. The adapter is comprised of a cone frustum and a cantilevered support structure (nicknamed the sugar scoop) to undergird the nozzle expansion surface. This geometry was received at Langley in late April 1996; with an aggressive model design and construction program using stereolithography and rapid prototyping techniques, 4.17% Hyper-X booster stack models were fabricated, and subsonic and hypersonic data on the launch configuration (castor/adaptor/free flyer) were obtained by late June. Booster performance and cost issues led to the abandonment of the Castor. The next candidate launch vehicle to be evaluated was the Orbital Sciences Corporation Pegasus.

Langley's Aerothermodynamics Branch had previously constructed 3% Pegasus models that had been modified to include both hybrid and XL Pegasus configurations as part of the Pegasus Return-to-Flight activity. Using rapid prototyping fabrication methods, both

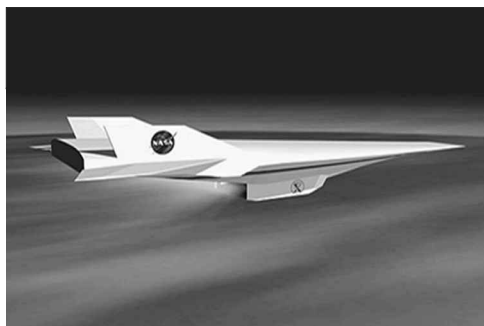


Fig. 1 Artist's representation of HXRV in flight.

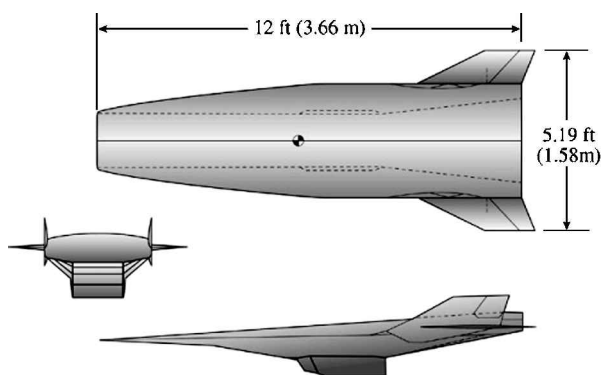


Fig. 2 Three-view drawing of the HXRV.

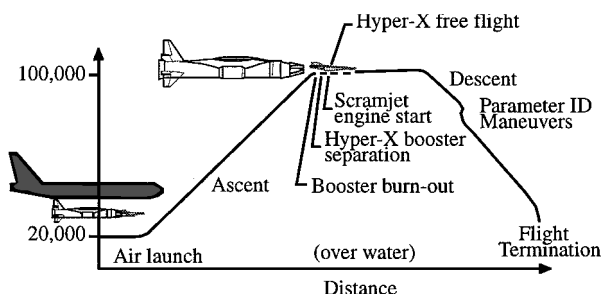


Fig. 3 Hyper-X flight profile.

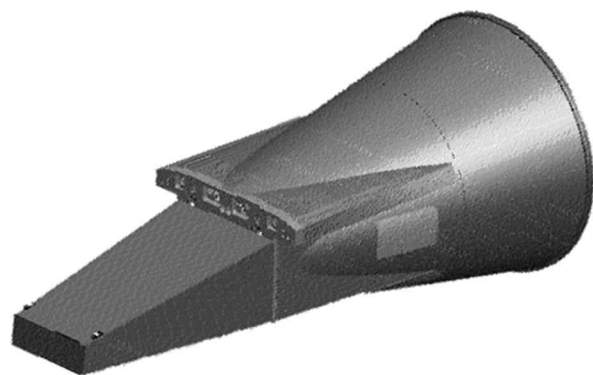


Fig. 4 Interstage adapter.

a 3% Hyper-X free flyer/adaptor forebody (preseparation) and an adapter-alone forebody (postseparation) were fabricated to fit the existing Pegasus model. Hypersonic tests at Mach 6 and 10 were conducted on the pre- and postseparation launch vehicle configurations in the late summer of 1996.

The first attempts at defining the hypersonic aerodynamic characteristics of the HXRV made use of a 12-in. (8.33%) keel line 3 model. The model was precision machined from stainless steel with variable rudder and full-flying wing deflection parametrics. The model was sting mounted through the expansion nozzle on a six-component strain gauge balance. In keeping with the multiuse design philosophy, this model was sized to permit an interstage adapter to be mounted to the sting at various axial locations and at

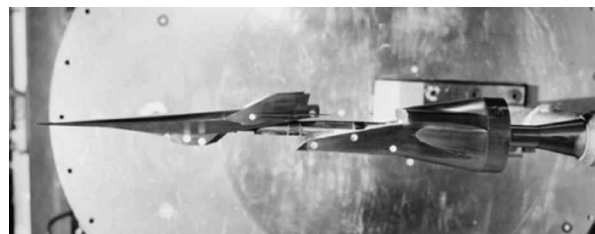


Fig. 5 Photograph of initial stage separation interference test setup in 31-Inch Mach 10 Tunnel.

two pitch orientations. Figure 5 is a setup photograph taken in the Langley 31-Inch Mach 10 Tunnel. Although the balance/sting assembly interferes with the flow between the HXRV and the adapter and permits only axial separations, this model provided an important preliminary assessment of the order of magnitude of the interference aerodynamics and aided in the development of required parametrics for the interference aerodynamics database. Tests were conducted at both Mach 6 and 10 to evaluate Mach-number effects on the hypersonic interference. These tests were completed in the fall of 1996, shortly after the release of the request for proposal (RFP). By early October (the date of the Hyper-X RFP release), over 20 weeks of wind-tunnel testing on 3% HXLV and 8.33% HXRV configurations had been concluded; these tests produced basic aerodynamic data as well as interference loads on the free flyer in proximity to the adapter. These data were used along with results calculated by engineering methods in a 3 + 3 degree-of-freedom simulation of the free flyer's motion relative to the Pegasus adapter during separation (simultaneous three-degree-of-freedom simulation of the free flyer and three-degree-of-freedom simulation of booster in close proximity). This effort by the Hyper-X stage separation team identified the axis systems and critical parameters required to define the relative motion of the two systems and identified a desired database of six-component force and moment data on both free flyer and Pegasus/adaptor at 40,000 different combinations of relative position, relative incidence, and free-flyer control settings. The volume of data required, the schedule, and possible cost led to the final conclusion that tests utilizing a captive trajectory system at high-Mach-number conditions were the only means of producing the volume of data in the scheduled time. This conclusion focused stage separation wind-tunnel testing activities on the Arnold Engineering and Development Center (AEDC), where the U.S. Air Force utilizes captive trajectory systems (CTS) for store separation tests at subsonic to hypersonic conditions<sup>7-9</sup> and where NASA developed its space-shuttle stage separation wind-tunnel database.<sup>10-13</sup> In addition, the relatively large size of the AEDC hypersonic tunnels is desirable for benchmark testing the full launch vehicle configuration. Cost remained an open issue and, while beyond the scope of this paper, led to a decrease in the size of the matrix ultimately to 26,000 points.

### Model Design Considerations

CTS were designed primarily for store separation studies. In such studies the main airframe is stationary in the tunnel at a given angle of attack and sideslip (internal strain gauge balance is blade mounted on a fixed strut), and the store (internal balance is sting mounted) is traversed behind the aircraft at a series of axial, lateral, and vertical positions and at relative pitch, yaw, and roll. With a database that bounds the relative positions of the vehicles in flight and has sufficient resolution, the trajectory of the store can be computed for any set of mass properties. Figure 6 is a schematic diagram showing this arrangement. In AEDC Tunnel B the CTS is mounted on top of the tunnel, and the primary model strut assembly is injected from beneath the tunnel floor. Therefore if the store separates from the lower surface of the carrier, models are tested inverted. This arrangement is shown in Fig. 7, a photograph of a conceptual two-stage reusable space transportation system installed in AEDC Tunnel B for CTS testing. The larger (and typically heavier) model is strut mounted, and the smaller (typically lighter) model (the store) is mounted to the CTS rig. CTS test procedure requires both models to be in the hot hypersonic flow for extensive periods of time ( $\geq 15$  min).

To provide internal room for a force balance and to protect it from thermal (high-temperature) effects, a free-flyer scale of 12-15%

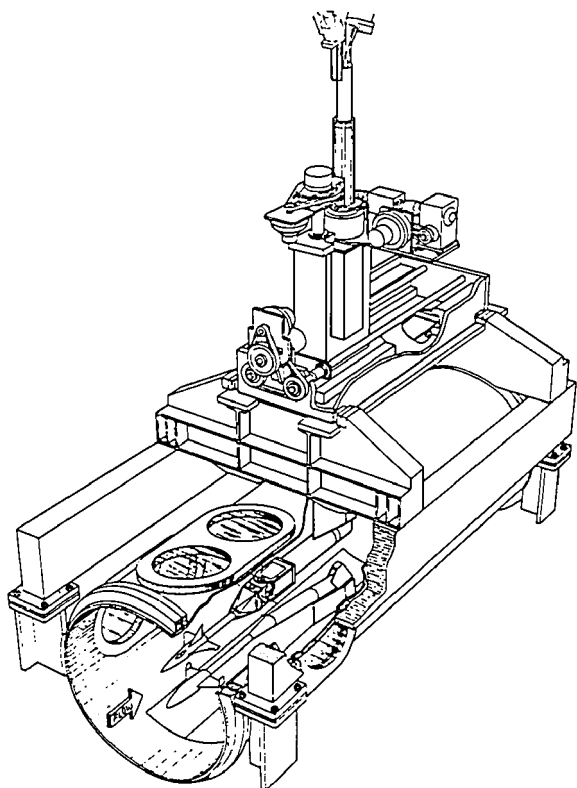


Fig. 6 Schematic diagram of two models mounted for CTS testing in AEDC Tunnel B.



Fig. 7 Photograph of conceptual two-stage space transportation system separation setup in AEDC Tunnel B.

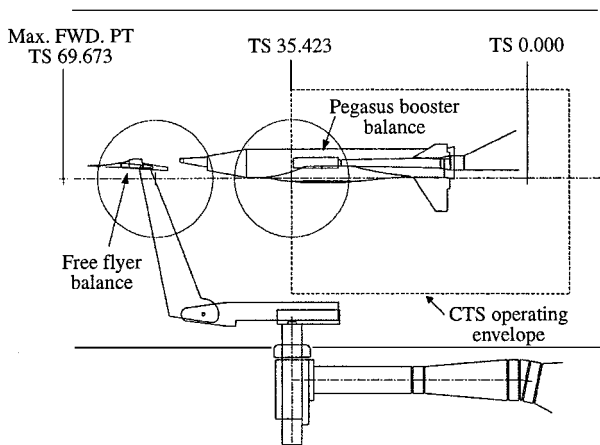


Fig. 8 Diagram of 8.33% Hyper-X stage separation hardware in AEDC Tunnel B.

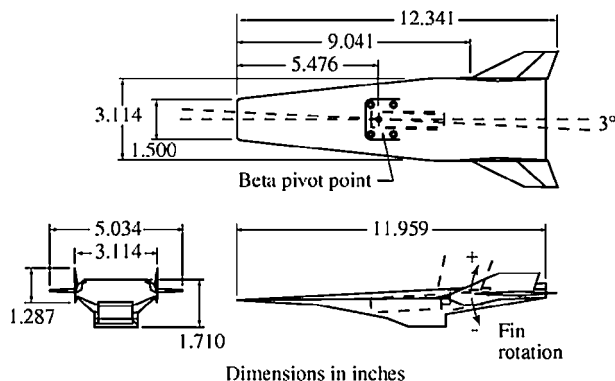


Fig. 9 Diagram of the model balance, blade support system for Hyper-X stage separation testing in AEDC Tunnel B.

was desired. Because of the predominantly axial orientation of the free flyer on the launch vehicle stack, the larger vehicle (Pegasus/adaptor) is mounted to the CTS, and the smaller vehicle (free flyer) is blade mounted to the strut system. Figure 8 is a schematic of this test setup in AEDC Tunnel B. Structural analysis of the loads from booster weight on the CTS rig revealed that the desired model scale of 12–15% exceeded safety factor load limits. A maximum model scale of 8.33% was possible only after the original model design was revised to minimum wall thickness for the heat load imposed by Tunnel B. The decision to maintain model scale at the expense of minimum wall thickness effectively eliminated the capability to reuse the model at a later date in Tunnel C (Mach 10) as a result of a heat load incompatibility.

This size limitation focused attention on the problem of locating a blade-mounted force balance in an 8.33% (12-in.-long) free flyer. Consideration was given to designing and fabricating a pancake-shaped balance, but there was concern that design, fabrication, calibration, and heat protection for such a balance in time to meet the required schedule was an unacceptable risk. There was an alternative. One active six-component balance in Langley’s inventory appeared small enough to fit within the outer mold lines of an 8.33% free flyer. Figure 9 is a sketch showing the location of SS02B balance in the model. The dashed rectangle parallel to the upper surface in the side view represents the body of the balance. The dashed trapezoid behind the dashed rectangle represents the block supporting the balance that has the cooling interface and is attached to the blade support (represented by the dashed lines above the side view). In the top view sideslip  $\beta$  was obtained by fabricating two balance blocks to be mounted in the free flyer: one with a balance bore aligned with the model and one with the balance bore at a 3-deg angle with respect the fuselage. This was necessary to keep the blade support unloaded in the lateral direction during testing and to keep the free flyer in the proper tunnel location relative to the Pegasus/adaptor. Because of space limitations, once the balance was assembled with the supporting block, blade interface cooling passages were connected directly to the block, essentially taking this balance out of service except for Hyper-X stage separation testing. This alternative also bore a risk because of the lack of a backup balance. Downtime caused by a balance failure (or worse, removal and later reinstallation of the CTS rig after balance repair) carried a significant cost risk. In spite of the cost risk, this alternative was accepted by the program over the fabrication of a new pancake balance, which bore technical, cost, and schedule risk.

The 3 + 3 degree-of-freedom simulation using engineering codes and available wind-tunnel data produced a sufficient number of collisions that an alternative stage separation mechanism was added to the test matrix for evaluation. This approach rotated the portion of the adaptor under the free-flyer nozzle down as separation occurred; the term “drop jaw” was applied to this adaptor design. Figure 10 is a three-view drawing of the final stage separation Pegasus/adaptor design incorporating the drop jaw. Drop jaw positions of 30, 60, and 90 deg were added to the baseline undeflected (0-deg) orientation and absorbed in the 26,000 point test matrix. The CTS test at AEDC began in November 1997.

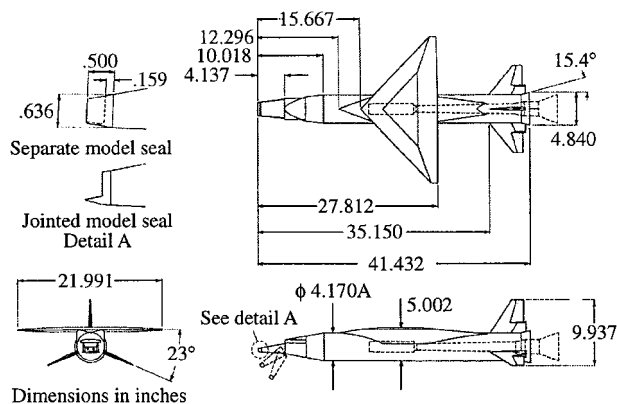


Fig. 10 Sketch of the 8.33% Hyper-X Pegasus Booster with variable drop jaw.

### Facilities

Because of its size and interface with a CTS system, the AEDC von Kármán Gas Dynamics Facility (VKF) Tunnel B became the primary test facility for stage separation. The Langley 20-Inch Mach 6 and 31-Inch Mach 10 tunnels, utilized in launch, postlaunch, and free-flyer hypersonic testing, were initially excluded from stage separation tests because their relatively small size could not accommodate a free flyer and the full length of booster at a scale large enough to house force and moment balances. Later, both of these facilities became indispensable in addressing concerns that could not be addressed in Tunnel B, including the effects of high heating to the free-flyer balance and blade support interference on free-flyer aerodynamics. Additionally, a comparison of the interference aerodynamics at Mach 6 and 10 was performed in the Langley facilities using the free flyer and the adapter portion of the booster model to establish a preliminary Mach 10 separation database.

#### AEDC VKF Tunnel B

Tunnel B is a continuous, closed-circuit variable density tunnel with an axisymmetric contoured nozzle and a 50-in.-diam test section. The test gas, dry air, is heated to avoid air liquefaction in the test section. Test conditions include a range of freestream unit Reynolds numbers from  $0.3 \times 10^6$  to  $4.7 \times 10^6$ /ft. Because the facility is capable of continuous operation for hours, balance heating can become an issue. Consequently, the NASA-supplied free-flyer balance and vertical strut were water cooled. Free-flyer angle-of-attack variations were obtained by manually changing a pivot and pin connection. Nominal free-flyer sideslip angles tested were 0 and  $-3$  deg. The Pegasus booster model was mounted to the CTS mechanism via an AEDC-supplied balance, water jacket, and straight sting combination. The CTS mechanism is a remote positioning six-degree-of-freedom, electromechanical drive system that can be installed on the top of AEDC Tunnels A, B, or C. The axial and vertical motions are obtained using linear drive units. Lateral motion is achieved by rotating the roll-pitch-yaw support arm about the vertical support arm at the vertical support axis with the aft yaw mechanism and compensating for the resulting yaw with the forward yaw mechanism. For additional information on Tunnel B and the CTS, see Refs. 14 and 15.

#### NASA Langley Research Center (LaRC) 20-Inch Mach 6 Tunnel

The NASA Langley 20-Inch Mach 6 tunnel is a blowdown facility with a 20 in.  $\times$  20 in. square test section that operates at a fixed Mach number of 6, using dry air as the test medium. Typical test conditions in this facility include nominal freestream unit Reynolds numbers from  $0.5 \times 10^6$  to  $9 \times 10^6$ /ft. Model angle of attack can be varied in a pitch-pause mode from  $-5$  to  $+55$  deg, depending on the length and position of the model in the test section. The design of the injection system permits the pitch-pause sequence at sideslip angles up to 5 deg. Run times are typically several minutes with a maximum time of approximately 15 min.

#### NASA LaRC 31-Inch Mach 10 Tunnel

The NASA Langley 31-Inch Mach 10 tunnel is also a blowdown facility, with a 31-in. square test section that operates at a fixed

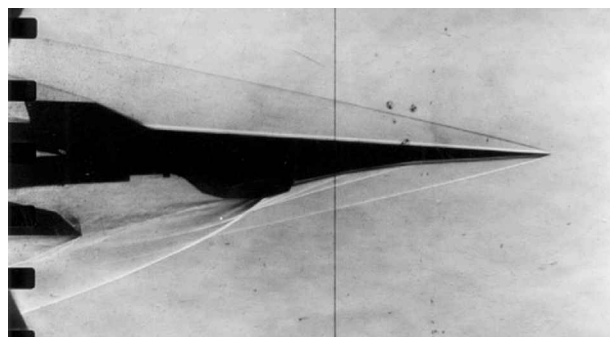
Mach number of 10, using dry air as the test medium. Typical test conditions in this facility include nominal freestream unit Reynolds numbers ranging from  $0.55 \times 10^6$  to  $2.15 \times 10^6$ /ft. Angle of attack can be varied  $\pm 45$  deg and runs last nominally 60 s. For additional information on both the 20-Inch Mach 6 Tunnel and the 31-Inch Mach 10 Tunnel, see Refs. 16 and 17.

### Representative Results and Discussion

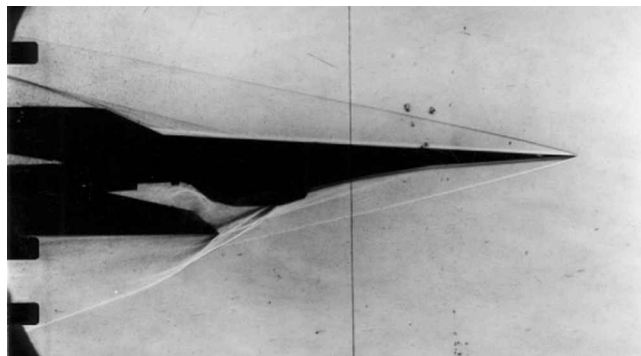
The stage separation wind-tunnel test program evolved from a low-cost component testing approach for preliminary order of magnitude screening of early separation concepts to benchmarking the full Pegasus booster/free-flyer mutual interference aerodynamics for the flight data book via captive trajectory system testing. Analysis of this data, including simulation results, led to follow-on testing for envelope expansion and risk reduction. This section provides representative results and discussion from each stage of this evolution.

#### Early Stage Separation Configuration Screening

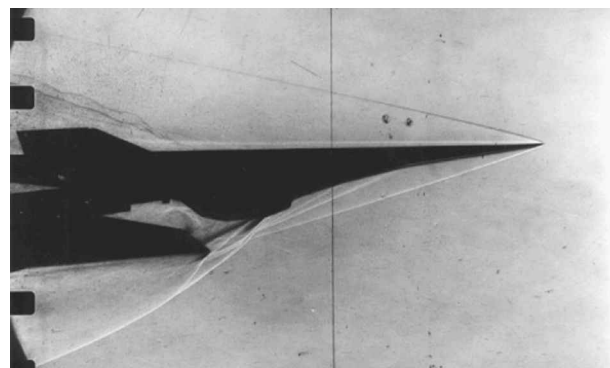
Figure 5 shows the 8.33% sting-mounted free flyer installed in the 31-Inch Mach 10 Tunnel. The interstage adapter, which mates the free flyer to the cylindrical fuselage of the booster, is clamped to the sting behind the free flyer. With this arrangement the axial location  $x_{sep}$  and pitch angle of the adapter relative to the sting  $\theta_{wt}$  could be varied. Figures 11a–11c are three schlieren photographs of the interference flowfield between the adapter and free flyer in the Langley



a)  $\alpha = 0$  deg,  $x_{sep} = -3.75$  ft,  $A_{sep} = -4$  deg



b)  $\alpha = 0$  deg,  $x_{sep} = -0.75$  ft,  $A_{sep} = -4$  deg



c)  $\alpha = 2$  deg,  $x_{sep} = -0.75$  ft,  $A_{sep} = -4$  deg

Fig. 11 Schlieren photographs of Mach 6 test partial separation hardware.

20-Inch Mach 6 Tunnel. Figure 11a shows the assembly at  $\alpha = 0$  deg with the adapter at a full-scale separation distance of 3.75 ft and a nose-down attitude of  $-4$  deg. The shock structure is well defined, and there appears to be a slip line coming off the engine and impacting the front of the adapter. Figure 11b shows the assembly at the same angle of attack with the adapter at a full-scale separation of 0.75 ft and the same nose-down attitude. A complex flow structure is noted between the adapter and the back of the engine package, and a separation shock is visible on the top of the free flyer ahead of the vertical fins. Figure 11c shows the assembly at 2-deg angle of attack with the components in the same relative positions as on Fig. 11b with an unsteady separation on the upper surface. These photographs show that the flowfield between the free flyer and the adapter possesses characteristics that range from a separated wake resembling a driven cavity to direct flow impingement on the free-flyer nozzle.

The influence of the interference on the aerodynamics of the free flyer is shown in Fig. 12. In Fig. 12a HXRV pitching-moment coefficient is plotted vs angle of attack for HXRV without the adapter (interference-free) and in the presence of the  $-4$  deg (nose-down) adapter at four different axial separations. The largest interference effect is for an axial separation of 0.75 ft (full scale), where a nose-down  $\Delta C_m$  on the order of  $-0.02$  was produced. There is a gradual reduction as axial separation is increased, and at full-scale separation distances of 3 and 3.75 ft angle of attack is shown to have a mitigating effect. (With increasing angle of attack, the gap between the nose-down adapter and the free flyer becomes more aligned with the freestream, which provides a relieving effect.) Figure 12b puts this interference in perspective by comparing interference-free maximum nose-down pitch control to the maximum interference

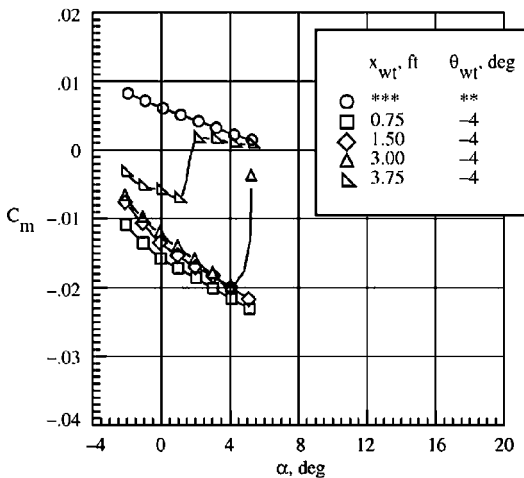


Fig. 12a Effect of axial separation distance between the HXRV and adapter on pitching-moment coefficient for  $A_{sep} = -4$  deg.

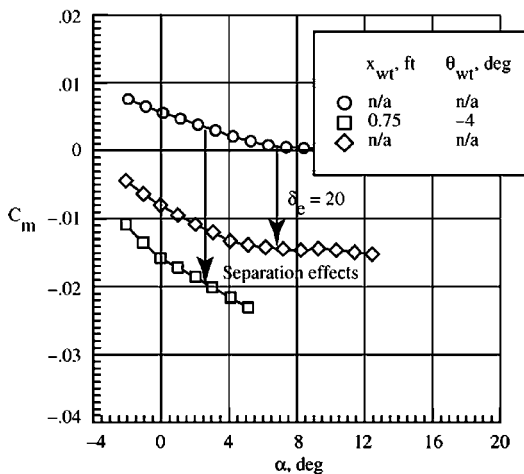


Fig. 12b Comparison between the effect of separation interference and control deflection on HXRV pitching-moment coefficient.

measured; the interference is equivalent to approximately 1.5 times the maximum control surface influence. These and other results obtained confirmed the need for detailed database development. Additionally these data were used in the 3 + 3 degree-of-freedom simulation that guided the test matrix design for the CTS test. The simulations also indicated little clearance between the adapter and the free flyer during separation, instigating incorporation of a drop jaw adapter as a variable in the test matrix.

**Captive Trajectory Testing**

Figure 13 is a setup photograph of the blade-mounted HXRV and the CTS-mounted Pegasus/adapter booster in AEDC Tunnel B. This shows the inverted orientation of the models and emphasizes the difference in size between the two models. For each block of wind-tunnel runs, the Pegasus was placed on centerline for Pegasus alone data, then retracted to the top of the tunnel so the HXRV could be injected from below for HXRV alone data. At this time the Pegasus was docked (brought into position) behind the HXRV and moved through its sequence of positions relative to the HXRV to obtain interference data on both vehicles. Each block of wind-tunnel runs was concluded with another set of HXRV alone data and booster alone data to allay concerns of balance heating effects on the HXRV during the 15-20 min of continuous exposure to the 900°R freestream. Repetition of this procedure for each block of runs provided numerous repeat data points to ensure measurement system stability throughout the test.

Figure 14 is a schlieren photograph of the interference flowfield with the drop jaw deflected to 60 deg. The flowfield is extremely complex with multiple shock interactions and compression waves produced in the area between the HXRV and the adapter. The effect of varying drop jaw angle on the free-flyer pitching-moment

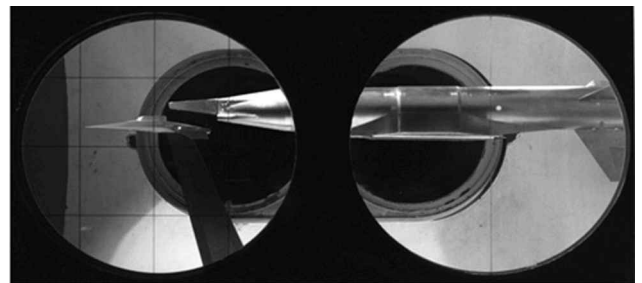


Fig. 13 Setup photograph of the Hyper-X stage separation hardware in AEDC Tunnel B.



Fig. 14 Schlieren photograph taken during Hyper-X stage separation testing in AEDC Tunnel B with the drop jaw at 60 deg,  $x_{sep} = -4$ ,  $A_{sep} = 0$  deg.

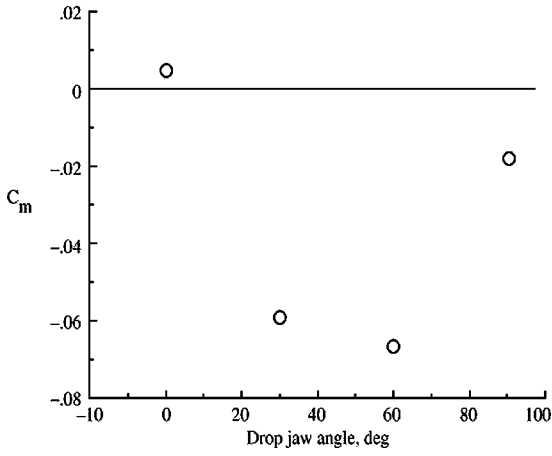


Fig. 15 Effect of adapter drop jaw angle on HXRv pitching-moment coefficient.

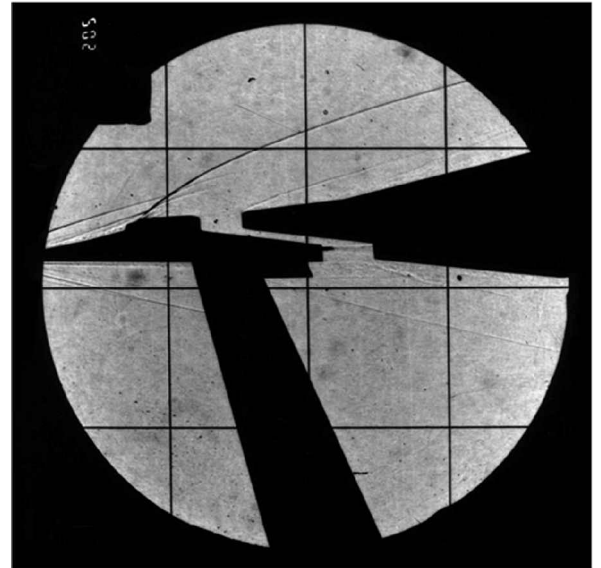


Fig. 16b Schlieren photograph from AEDC Tunnel B Mach 6 separation tests for  $A_{sep} = 0$  deg,  $x_{sep} = -20$ .

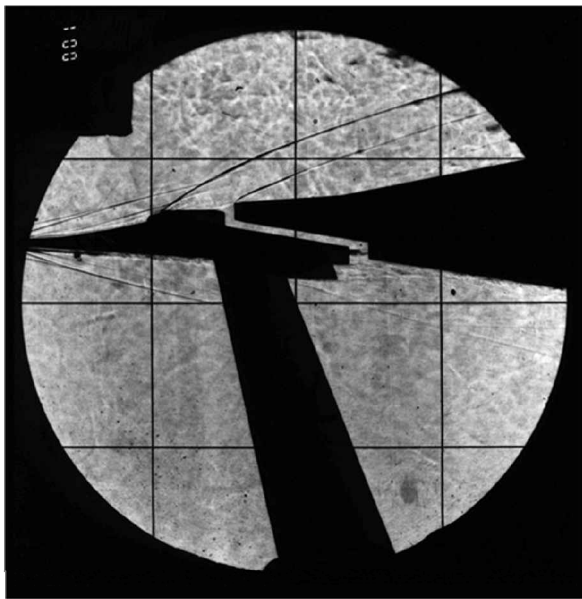


Fig. 16a Schlieren photograph from AEDC Tunnel B Mach 6 separation tests for  $A_{sep} = 0$  deg,  $x_{sep} = -9$ .

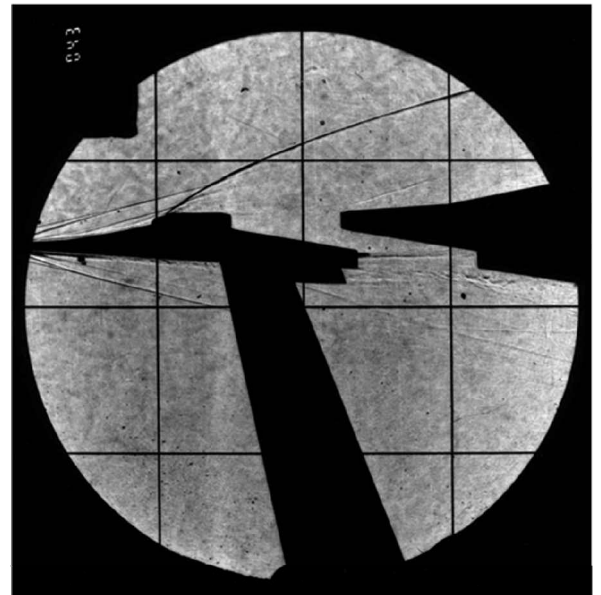


Fig. 16c Schlieren photograph from AEDC Tunnel B Mach 6 separation tests for  $A_{sep} = 0$  deg,  $x_{sep} = -44$ .

coefficient is shown in Fig. 15. Increasing the drop jaw angle pressurizes the free-flyer nozzle and produces a nose-down moment. Over the drop jaw angles tested, the maximum influence is found at a 60-deg deflection. These data were used in the 6 + 6 degree-of-freedom simulations, which demonstrated that the drop jaw adapter generated nose-down pitching-moment inputs that could not be controlled by the control system. These results precipitated the decision not to deploy the drop jaw in flight, i.e., to fix the adapter at 0 deg.

Figure 16 is a series of schlieren photographs from AEDC Tunnel B for a purely axial separation (no lateral or vertical translation, no relative pitch, yaw, or roll) at separation distances from 9 to 44 in. full scale. Compared to the complex flowfield found with the 60-deg drop jaw deflection, the flowfield between the HXRv nozzle and the adapter is characterized by a relatively benign wake flow interaction. Figure 17 demonstrates interference effects on pitching-moment coefficients approximately an order of magnitude smaller than the 60-deg drop jaw deflection for a purely linear separation at free-flyer angles of attack of 0 and 3 deg over a range of  $x_{sep}$ . These results along with all test data for fixed adapter geometry (0-deg drop jaw) were used to produce the database for control system design for the separation sequence between the HXRv and the booster. AEDC has a safety requirement that prohibits the store on the CTS from coming closer than 0.25 in. to the strut-mounted vehicle. This is equivalent to a minimum full-scale separation distance of 3 in.;

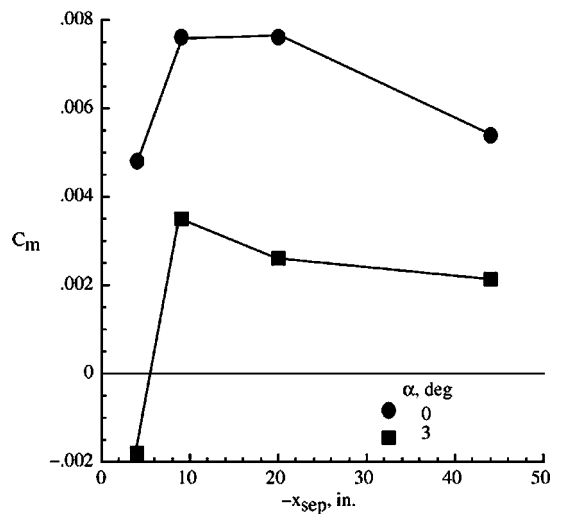


Fig. 17 Effect of axial separation distance on HXRv pitching-moment coefficient,  $A_{sep} = 0$  deg,  $z_{sep} = 0$ .

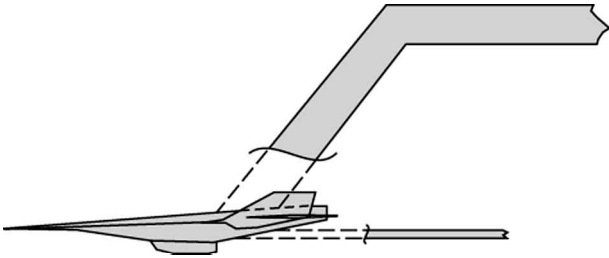


Fig. 18 Schematic representation of the testing technique to determining blade and sting interference effects.

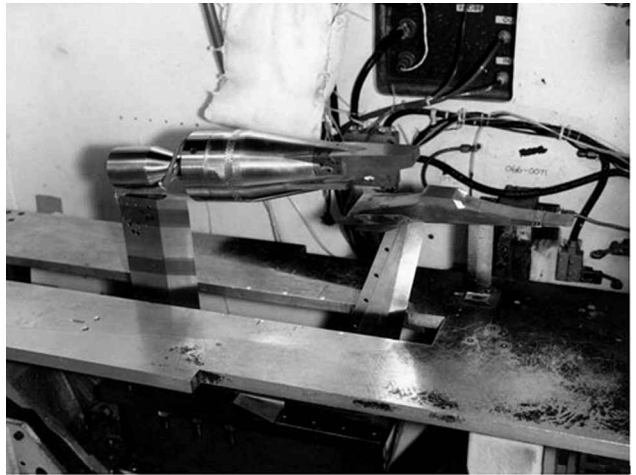


Fig. 20 Setup photograph of stage separation hardware test in the Langley 20-Inch Mach 6 Tunnel.

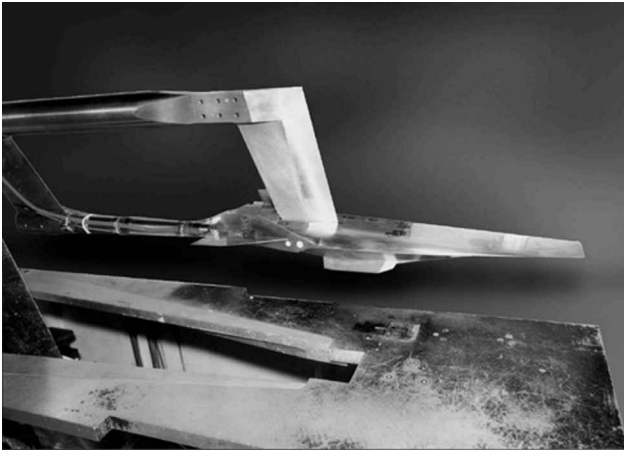


Fig. 19 Setup photograph of blade/sting interference test hardware in the Langley 20-Inch Mach 6 Tunnel.

the original test matrix was modified to accommodate this requirement and some desired orientations removed. Additionally concerns about HXRV balance heating were not unfounded; late in the test the yaw beam was lost as a result of heat. Time and funding constraints caused other modifications to the test plan, but in the final analysis 96% of the 26,000+ point test matrix was completed. Several stage separation issues remained to be resolved: defining the effect of the blade support on HXRV data, determining interference effects at distances closer than 3 in., and determining Mach 10 interference effects.

#### Blade/Sting Interference Risk Reduction Testing

A 12.5% model was fabricated to develop the stability and control database for smaller control increments than was possible with the 8.33% model. Additionally, multiple mount capability for blade/sting interference was designed into this model. Figure 18 shows schematically the approach to defining sting interference at hypersonic conditions. A model is tested supported by a sting alone and a blade alone. Deltas are provided by testing with dummy (non-metric) blade while sting supported and a dummy (nonmetric) sting when blade supported. Figure 19 is a photograph of the model sting mounted with a dummy blade in the Langley 20-Inch Mach 6 Tunnel. These tests successfully defined the support interference effects and were used to correct all HXRV data for support effects, not just the stage separation results. Details are presented in Ref. 6.

#### Envelope Expansion Testing

Balance heating problems encountered during the Mach 6 stage separation test emphasized the improbability of successfully conducting Mach 10 stage separation tests at AEDC on the 8.33% model. The severity of the heating environment is nearly double at Mach 10 compared to Mach 6. Therefore, to bridge the gap from Mach 6 to 10, a support system was designed and fabricated to interface with the Langley 31-Inch Mach 10 and 20-Inch Mach 6 tunnels. This system supports the HXRV model from the AEDC test on a blade identical to the AEDC blade in proximity of the adapter portion of the booster model from the AEDC test. Figures 20 and 21

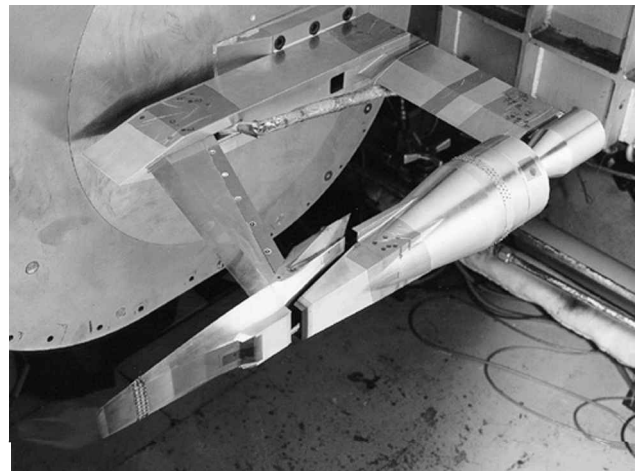


Fig. 21 Setup photograph of stage separation hardware in the Langley 31-Inch Mach 10 Tunnel.

are setup photographs of this test article in the 20-Inch Mach 6 and 31-Inch Mach 10 tunnels, respectively. Besides providing information on the differences between Mach 6 and 10 interference data, this apparatus presented the opportunity to expand the test envelope from the AEDC test to include proximities closer than permitted at AEDC. The data comparing Mach 6 and 10 are still under analysis. The Mach 6 results at closer separation distances have been included in the multi-degree-of-freedom separation database used to design the control system to promote collision-free separation.

Monte Carlo simulations were run as the database was being constructed, with each new test series contributing as the data became available. An initial 500-run simulation was conducted and used to identify collision conditions. (Efforts such as these identified the out-of-control pitching moments induced by the drop jaw that resulted in the fixed jaw requirement for the first flight.) Concerns about the AEDC data not “bounding” the simulations created the necessity of modifying the Mach 6 vs Mach 10 test apparatus and performing additional tests to reduce risk through further envelope expansion. Figures 22a–22g present the recent results of 100 collision-free simulations based on the current database. The boxes represent the bounds of the test data with the heavy vertical lines indicating the same bounds based on the AEDC data alone. As the solid curves move outside the boxes, extrapolated data are used. The simulations are anchored at  $x_{sep} = -70$  in. by the interference-free data on the HXRV. The role of computational fluid dynamics in augmenting the separation database as well as developing a correlation parameter for data extrapolation is presented in Ref. 18.

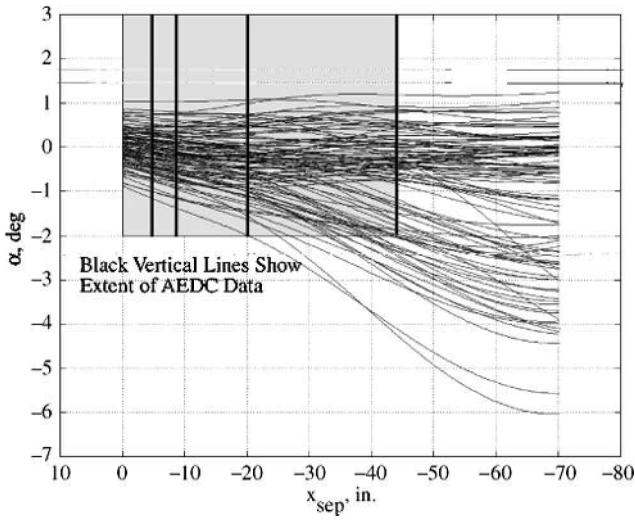


Fig. 22a Monte Carlo simulations of HXRV angle of attack with separation distance from the adapter.

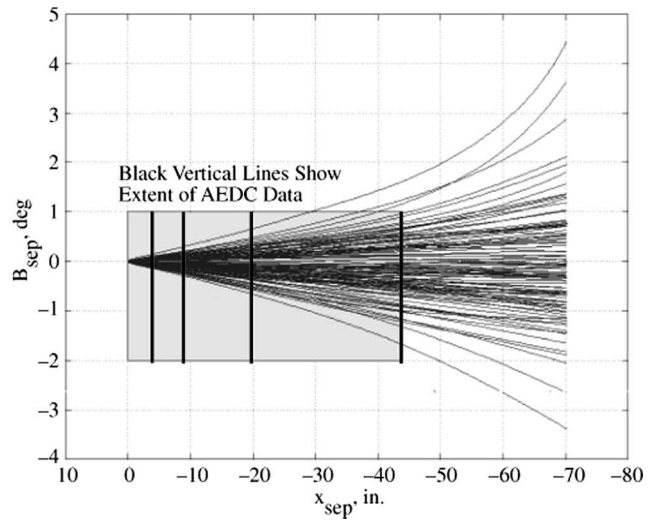


Fig. 22d Monte Carlo simulations of  $B_{sep}$  with separation distance from the adapter.

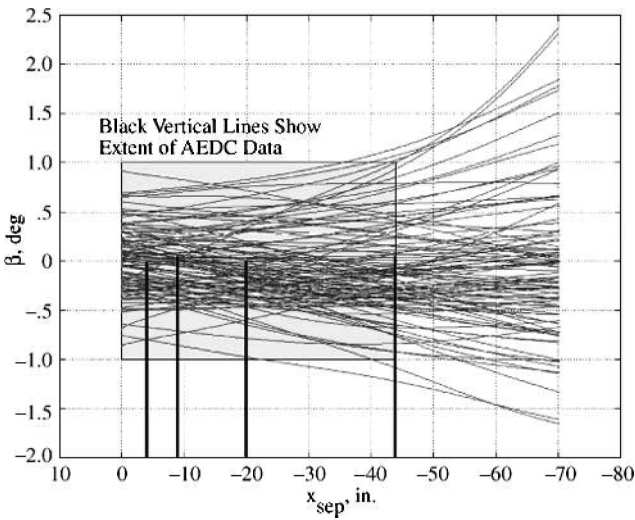


Fig. 22b Monte Carlo simulations of HXRV sideslip with separation distance from the adapter.

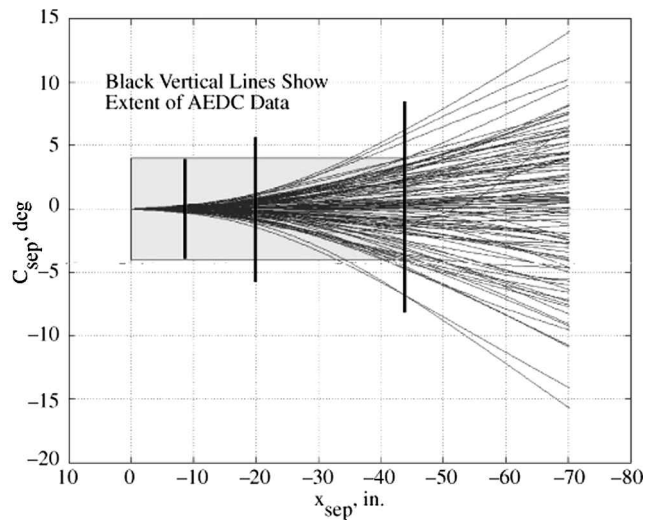


Fig. 22e Monte Carlo simulations of  $C_{sep}$  with separation distance from the adapter.

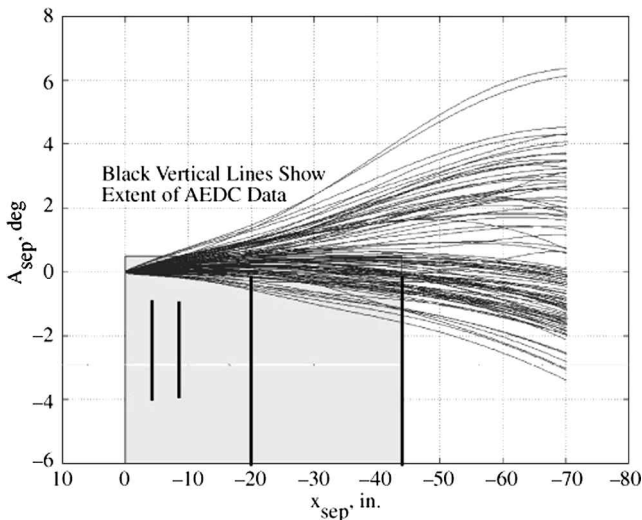


Fig. 22c Monte Carlo simulations of  $A_{sep}$  with separation distance from the adapter.

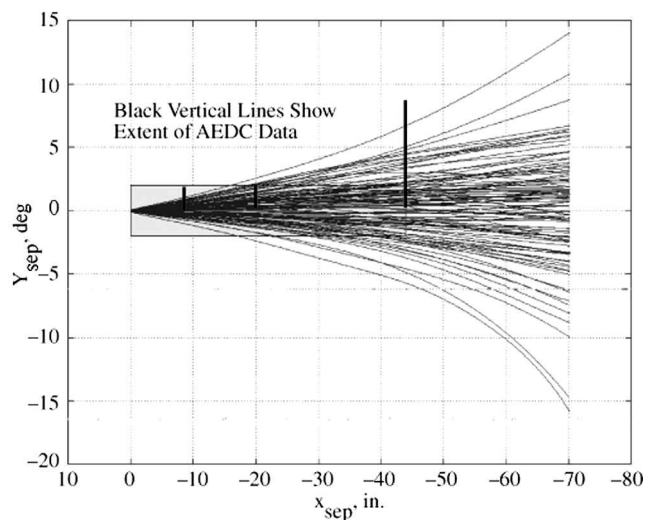


Fig. 22f Monte Carlo simulations of  $y_{sep}$  with separation distance from the adapter.

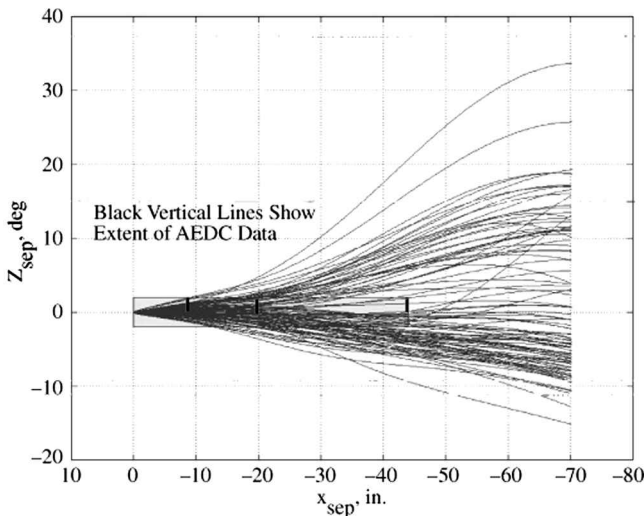


Fig. 22g Monte Carlo simulations of  $z_{\text{sep}}$  with separation distance from the adapter.

### Conclusions

The Hyper-X Research Vehicle is a 12-ft long, 2700-lb technology demonstrator designed to flight demonstrate for the first time a fully airframe-integrated scramjet propulsion system. Prior to the engine test, the vehicle must be boosted to test point and separated from the booster at high Mach number and high dynamic pressure conditions. The HXRV shape is not readily adaptable to a launch vehicle and requires an interface adapter. This nonaxisymmetric separation from the booster/adapter at extreme conditions is critical to the success of the mission. This paper has reviewed the Hyper-X stage separation wind-tunnel test program, including early planning, preliminary separation configuration screening, development of the database requirements, and captive trajectory testing. Sample test results have been provided, and risk reduction and envelope expansion follow-on testing have been reviewed. Results from simulations using these data have also been discussed. Although all of the dispersions from the nominal separation trajectory could not be completely bounded, the available facilities and test techniques (supplemented with computational fluid dynamics) have been used to produce the most extensive separation database possible. Monte Carlo simulations using this database along with a model of the mechanical process have been used to develop control systems to produce clear separations at minimum risk.

### Acknowledgments

The authors wish to recognize the large team of individuals that contributed to defining this test program and assisting in its implementation: first and foremost Mary Kae Lockwood, Scott Striepe, and Eric Queen for early definition of the critical parameters and separation simulations defining the extreme difficulty of the problem; Ravi Dhanvada, Chris Tarkenton, and the MicroCraft, Hampton, Virginia, team for the design and fabrication of hardware and models; Walt Engelund, Charles Cockrell, Doug Dilley, Peter Pao, Pieter Buning, and Tin Chee Wong for continuing dialog on the pros and cons of the test program from both the experimental and computational viewpoint; B. F. Tamrat (Boeing Seal Beach) for his continued input and his participation and support of the testing process; John Martin and his colleagues for applying the data to produce clean separation simulations; the testing team and the shops at AEDC for their performance in conducting the test and producing the data; the technicians and data reduction staff of the 20-Inch Mach 6 and 31-Inch Mach 10 Tunnels for their performance in conducting the preliminary and follow-on risk reduction testing; David Roberts and

the machine shop at Langley Research Center for countless on-site modifications of hardware without which the necessary tests could not have been accomplished; and last but not least Dave Reubush, Hyper-X stage separation manager, for his interaction with the U.S. Air Force, various separation tiger teams, and MicroCraft on funding and hardware issues so the experimentalists could focus on the test process.

### References

- Rausch, V. L., McClinton, C. R., and Hicks, J. W., "NASA Scramjet Flight to Breathe New Life into Hypersonics," *Aerospace America*, Vol. 35, No. 7, 1997, pp. 40–42, 45, 46.
- Rausch, V. L., McClinton, C. R., and Crawford, L., "Hyper-X: Flight Validation of Hypersonic Airbreathing Technology," International Symposium on Air Breathing Engines, Paper 97-7024, Sept. 1997.
- Hunt, J. L., and Eiswirth, E. A., "NASA's Dual-Fuel Airbreathing Hypersonic Vehicle Study," AIAA 96-4591, Nov. 1996.
- Bogar, T. J., Alberico, J. F., Johnson, D. B., Espinosa, A. M., and Lockwood, M. K., "Dual-Fuel Lifting Body Configuration Development," AIAA 96-4592, Nov. 1996.
- Holland, S. D., Woods, W. C., and Engelund, W. C., "Hyper-X Research Vehicle Experimental Aerodynamics Test Program Overview," *Journal of Spacecraft and Rockets*, Vol. 38, No. 6, 2001, pp. 828–835.
- Engelund, W. C., Holland, S. D., Cockrell, C. E., Jr., and Bittner, R. D., "Aerodynamic Database Development for the Hyper-X Airframe-Integrated Scramjet Propulsion Experiments," *Journal of Spacecraft and Rockets*, Vol. 38, No. 6, 2001, pp. 803–810.
- Carman, J. B., Jr., "Store Separation Testing Techniques at the Arnold Engineering Development Center—Volume I: An Overview," Arnold Engineering Development Center, AEDC-TR-79-1, Arnold AFB, TN, Aug. 1980.
- Carman, J. B., Jr., Hill, D. W., Jr., and Christopher, J. P., "Store Separation Testing Techniques at the Arnold Engineering Development Center—Volume II: Description of Captive Trajectory Store Separation Testing in the Aerodynamic Wind Tunnel (4T)," Arnold Engineering Development Center, AEDC-TR-79-1, Arnold AFB, TN, June 1980.
- Billingsley, J. P., Burt, R. H., and Best, J. T., Jr., "Store Separation Testing Techniques at the Arnold Engineering Development Center—Volume III: Description and Validation of Captive Trajectory Store Separation Testing in the von Karman Facility," Arnold Engineering Development Center, AEDC-TR-79-1, March 1979.
- Daileda, J. J., and Marroquin, J., "Results of SRB Separation Tests Using the 0.010 Scale SSV Model 75-OTS in the AEDC VKF Tunnel A (IA143)—Volume 1," NASA CR-151401, Feb. 1978.
- Daileda, J. J., and Marroquin, J., "Results of SRB Separation Tests Using the 0.010 Scale SSV Model 75-OTS in the AEDC VKF Tunnel A (IA143)—Volume 2," NASA CR-151402, Feb. 1978.
- Daileda, J. J., and Marroquin, J., "Results of SRB Separation Tests Using the 0.010 Scale SSV Model 75-OTS in the AEDC VKF Tunnel A (IA143)—Volume 3," NASA CR-151403, Feb. 1978.
- Daileda, J. J., and Marroquin, J., "Results of SRB Separation Tests Using the 0.010 Scale SSV Model 75-OTS in the AEDC VKF Tunnel A (IA143)—Volume 4," NASA CR-151404, Feb. 1978.
- Test Facilities Handbook*, 13th ed., von Karman Gas Dynamics Facility, Vol. 3, Arnold Engineering Development Center, Arnold AFB, TN, May 1992.
- Buchanan, T. D., and Crosby, W. A., "Captive Trajectory System Test Planning Information for AEDC Supersonic Wind Tunnel A and Hypersonic Wind Tunnels B and C," Arnold Engineering Development Center, AEDC-TR-83-40, Arnold AFB, TN, Dec. 1983.
- Miller, C. G., III, "Langley Hypersonic Aerodynamic/Aerothermodynamic Testing Capabilities—Present and Future," AIAA 90-1376, June 1990.
- Penaranda, F. E., and Freda, M. S., "Aeronautical Facilities Catalogue—Volume I: Wind Tunnels," NASA RP-1132, Jan. 1985.
- Buning, P. G., Wong, T.-C., Dilley, A. D., and Pao, J. L., "Computational Fluid Dynamics Prediction of Hyper-X Stage Separation Aerodynamics," *Journal of Spacecraft and Rockets*, Vol. 38, No. 6, 2001, pp. 820–827.